© 2019. Published by The Company of Biologists Ltd | Development (2019) 146, dev183905. doi:10.1242/dev.183905

RESEARCH REPORT

Conditional effects of the epigenetic regulator JUMONJI 14 in *Arabidopsis* root growth

Pietro Cattaneo*, Moritz Graeff*, Petra Marhava and Christian S. Hardtke‡

ABSTRACT

Methylation of lysine 4 in histone 3 (H3K4) is a post-translational modification that promotes gene expression. H3K4 methylation can be reversed by specific demethylases with an enzymatic Jumonji C domain. In *Arabidopsis thaliana*, H3K4-specific JUMONJI (JMJ) proteins distinguish themselves by the association with an F/Y-rich (FYR) domain. Here, we report that *jmj14* mutations partially suppress reduced root meristem size and growth vigor of *brevis radix* (*brx*) mutants. Similar to its close homologs, *JMJ15*, *JMJ16* and *JMJ18*, the *JMJ14* promoter confers expression in mature root vasculature. Yet, unlike *jmj14*, neither *jmj16* nor *jmj18* mutation markedly suppresses *brx* phenotypes. Domain-swapping experiments suggest that the specificity of JMJ14 function resides in the FYR domain. Despite *JMJ14* promoter activity in the mature vasculature, *jmj14* mutation affects root meristem size. However, JMJ14 protein is observed throughout the meristem, suggesting that the *JMJ14* transcript region contributes substantially to the spatial aspect of *JMJ14* expression. In summary, our data reveal a role for JMJ14 in root growth in sensitized genetic backgrounds that depends on its FYR domain and regulatory input from the *JMJ14* cistron.

KEY WORDS: *Arabidopsis*, Root, JMJ14, BRX, OPS, Phloem

INTRODUCTION

The nuclear DNA of eukaryotes is packaged as chromatin, the constitutive unit of which is the nucleosome, which is ∼146 base pairs of DNA wrapped around a core histone hetero-octamer (Kouzarides, 2007). Chromatin 'openness', and thus its accessibility for gene expression regulators, depends on covalent post-translational modifications at the protruding N-terminal tails of histones 3 (H3) and 4 (H4) (Kouzarides, 2007; Mosammaparast and Shi, 2010). These reversible modifications include the histone methylation state, which strongly influences gene expression levels and is controlled by specific methylases and demethylases (Kouzarides, 2007; Mosammaparast and Shi, 2010). Such methylation occurs at specific lysine (K) residues and the combinatorial methylation state determines the efficacy of transcription initiation, elongation and termination. For example, H3K9 and H3K27 methylation generally inhibit gene expression, whereas H3K4 and H3K36 methylation generally activate transcription. Moreover, there is a quantitative impact of methylation level, which ranges from mono- to trimethylation and is typically catalyzed by SET domain-containing proteins (Kouzarides, 2007; Mosammaparast and Shi, 2010). Trimethylated H3K4 (H3K4^{me3}) is most associated with transcribed genes, because it recruits activated RNA polymerase II to their 5′ end (Bannister and Kouzarides, 2005; Kouzarides, 2007). Lysine demethylation is catalyzed by various enzymes, which do not act on all methylation states (Bannister and Kouzarides, 2005; Kouzarides, 2007; Shi et al., 2004). Removal of methyl groups from trimethylated histone lysines is performed by proteins that contain a catalytic Jumonji C (JmjC) domain, which can also reduce other methylation states (Klose et al., 2006a,b; Tsukada et al., 2006). JmjC domain proteins can be sorted into distinct classes according to the presence of other conserved domains, which appear to determine specificity for a given histone methyl-lysine (Klose et al., 2006a).

The histone modification machinery is conserved in eukaryotes. For example, the genome of the model plant *Arabidopsis thaliana* encodes 21 JmjC domain-containing proteins, which can be grouped according to their overall structure and the presence of additional domains, features that likely confer specificity as well as promiscuity (Hong et al., 2009; Lu et al., 2008). For example, JMJ11 (also known as EARLY FLOWERING 6) and JMJ12 (also known as RELATIVE OF EARLY FLOWERING 6) contain additional JmjN and zinc-finger domains and target H3K27 and H3K9 (Lu et al., 2011; Yu et al., 2008), whereas the smaller JMJ30 and JMJ32 proteins contain no additional conserved domains and are specific for H3K27 (Gan et al., 2014; Lu et al., 2008). One group of proteins, comprising JMJ14, JMJ15, JMJ16 and JMJ18, is particular in that its members contain a phenylalanine- and tyrosine-rich, so-called FYR domain. The FYR domain is formed by the FYR-N and FYR-C subdomains, which constitute a single-folded functional module (García-Alai et al., 2010). Association of a JmjC domain with an FYR domain is apparently only found in plants (Klose et al., 2006a; Lu et al., 2008). Interestingly, the FYR domain is typical for TRITHORAX proteins, which are H3K4-specific methyltransferases (García-Alai et al., 2010; Klose et al., 2006a; Lu et al., 2008; Saleh et al., 2008). Matching this observation, H3K4-specificity has been demonstrated for JMJ14, JM15 and JMJ18 (Lu et al., 2010; Yang et al., 2012a,b).

In *A. thaliana*, histone demethylases have been mostly implicated in life-cycle transitions, notably flowering time (Gan et al., 2014; Greenberg et al., 2013; Jeong et al., 2009; Ko et al., 2010; Lu et al., 2010; Searle et al., 2010; Yang et al., 2012a,b). For example, *JMJ14*, *JMJ15* and *JMJ18* all affect flowering. However, genetic loss- and gain-of-function scenarios suggest functional diversification within this group despite the similarity of the encoded proteins. Whereas *jmj14* loss-of-function mutants flower early (Greenberg et al., 2013; Jeong et al., 2009; Lu et al., 2010; Searle et al., 2010), *jmj15* mutants have no flowering phenotype (Yang et al., 2012b) and *jmj18* mutants flower slightly late (Yang et al., 2012a). Moreover, *JMJ15* or *JMJ18* ectopic over-expression

Department of Plant Molecular Biology, University of Lausanne, Biophore Building, CH-1015 Lausanne, Switzerland.
*These authors contributed equally to this work.

‡Author for correspondence (christian.hardtke@unil.ch)

C.S.H., 0000-0003-3203-1058

Received 14 August 2019; Accepted 18 November 2019

Development (2019) 146, dev183905. doi:10.1242/dev.183905

triggers early flowering (Yang et al., 2012a,b), suggesting that *JMJ14* and *JMJ15/18* act antagonistically. *JMJ14* has also been implicated in post-transcriptional gene silencing (Le Masson et al., 2012), as a downstream component in the cell-to-cell spread of a mobile RNA silencing signal (Searle et al., 2010) that is directly linked to H3K4 methylation (Greenberg et al., 2013). Here, we provide evidence for a role of *JMJ14* in *A. thaliana* root growth.

RESULTS AND DISCUSSION

The phloem of higher plants is an essential tissue that delivers phloem sap from source to sink organs via sieve tubes (Lucas et al., 2013). Sieve tubes are formed by interconnected, enucleated sieve elements that are metabolically supported by their neighboring companion cells. The growth regions of plants, the apical meristems, connect to the mature phloem network via protophloem. For example, in *A. thaliana* root tips, two protophloem strands transfer phloem sap into the meristem to support cellular growth and proliferation driven by the stem cell niche. Impaired protophloem differentiation results in discontinuous sieve tubes, and thus suboptimal phloem sap delivery. Consequently, root meristem size and root growth are strongly reduced, and this is accompanied by other secondary systemic defects (Anne and Hardtke, 2017). This phenotype is for instance observed in *brevis radix* (*brx*) or *octopus* (*ops*) mutants, in which protophloem sieve elements frequently fail to differentiate and appear as morphological 'gaps' (Rodriguez-Villalon et al., 2014). Gap frequency can be used as a proxy for phenotypic severity.

JMJ14 mutation partially suppresses *brx* phenotypes

A forward genetic screen identified second site mutations that suppress the strongly reduced root growth of *brx* mutants (Depuydt et al., 2013). Besides loss-of-function mutations in BARELY ANY MERISTEM 3 (BAM3) [a receptor kinase that senses the secreted CLAVATA3/EMBRYO SURROUNDING REGION-RELATED 45 (CLE45) peptide], which fully suppress the *brx* phenotype (Depuydt et al., 2013; Hazak et al., 2017), a number of partial suppressors were isolated. For instance, loss of function in BIG BROTHER (BB) (an E3 ubiquitin ligase) partially rescues *brx* and also *ops* mutant phenotypes (Cattaneo and Hardtke, 2017). Whole-genome sequencing of bulked segregants (Kang and Hardtke, 2016) from another partial suppressor, line 2.91.1 (Depuydt et al., 2013) (Fig. 1A), suggested a point mutation in *JMJ14* (At4g20400) as the causative locus. This second site mutation occurred at the splice junction between intron 10 and exon 11 (Fig. 1B). Sanger sequencing of cDNA fragments that encompassed exons 9 to 12 confirmed the annotated transcript in wild type, whereas intron 10 was retained in *jmj14* mutant cDNA (Fig. 1C). This leads to the addition of two new amino acids after amino acid 780 and a subsequent premature stop codon at the end of the FYR-N subdomain, thus resulting in truncated JMJ14 protein that lacks the FYR-C subdomain. We named this allele *jmj14-4*, to distinguish it from previously published *jmj14-1* and *jmj14-2* T-DNA insertion alleles, and the *jmj14-3* point mutant (Searle et al., 2010).

To test whether *jmj14-4* represents a loss-of-function mutation, we crossed the *jmj14-1* mutant, in which *JMJ14* is disrupted by a T-DNA insertion in exon 6 (Searle et al., 2010), to *brx*. Similar to *brx jmj14-4* double mutants, root growth was partially restored in *brx jmj14-1* double mutants (Fig. 1A,D; Fig. S1A). Moreover, introduction of a transgene in which the *JMJ14* genomic sequence was expressed under control of the *JMJ14* promoter (*JMJ14::gJMJ14*) into *brx jmj14-4* or *brx jmj14-1* double mutants reverted their phenotype (Fig. 1E). These results prove that *JMJ14* loss-of function partially suppresses *brx* phenotypes, and that the FYR-C subdomain is essential for JMJ14 function, likely by guiding JMJ14 to the correct H3K4 targets (Klose et al., 2006a).

The *JMJ14* impact on root growth manifests in genetically suboptimal conditions

Despite partial rescue of macroscopic *brx* phenotypes, protophloem continuity was not restored in *brx jmj14* double mutants (Fig. 1F). Consistently, phloem-mediated translocation of carbofluorescin diacetate (CFDA) was not enhanced in *brx jmj14* mutants compared with *brx* mutants (Fig. 1G). These results suggest that *JMJ14* mutation suppresses the *brx* short root phenotype in a protophloem-independent manner, similar to what has been observed for *BB* mutation (Cattaneo and Hardtke, 2017). Partial rescue of *brx* by *bb* has been attributed to increased root meristem size, which is caused by enhanced meristematic cell proliferation, accompanied by mildly enhanced mature cell length. Rescue by *jmj14* was largely similar, in that meristem size was restored to wild type in terms of meristematic cortex cell number (Fig. 1H) and mature cortex cell length was increased compared with *brx* single mutants (Fig. 1I). Yet unlike *bb* mutation, *jmj14* mutation did not compensate for the slightly reduced formative divisions in *brx* (Rodriguez-Villalon et al., 2014) (Fig. 1J). Excess formative divisions that slow down root growth are thought to be responsible for the absence of enhanced root elongation in *bb* single mutants despite their bigger meristem (Cattaneo and Hardtke, 2017). By contrast, no significant difference in formative divisions, meristematic divisions or mature cell length were observed in *jmj14* single mutants compared with Col-0 (Fig. 1H-J). Thus, *jmj14* roots appeared entirely wild type, and a contribution of *JMJ14* to root growth vigor was only evident in the *brx* background. To test whether this was a generic feature, we created *jmj14-1 ops* double mutants. Their phenotype was essentially similar to that of *brx jmj14-1* double mutants (Fig. S1B-E), including secondary features such as lateral root density (Fig. 2A; Fig. S1F). We thus conclude that *JMJ14* inhibits root meristem activity upon suboptimal root growth in tissue culture.

JMJ14 mutation does not alter key physiological features of *brx*

Matching protophloem-independent rescue by *jmj14*, physiological features of *brx* were largely retained in *brx jmj14* double mutants. For instance, *JMJ14* mutation did not act through dampening of the CLE45/BAM3 pathway hyperactivity in *brx* (Breda et al., 2019; Depuydt et al., 2013), as *brx jmj14* double as well as *jmj14* single mutants were fully CLE45 sensitive (Fig. 2B). Also, the reduced auxin activity in *brx* meristems (Gujas et al., 2012; Mouchel et al., 2006) was not markedly restored in *brx jmj14* double mutants (Fig. 2C). Nevertheless, *brx jmj14* root growth could not be further enhanced by brassinolide treatment, which (partially) rescues auxin response and root growth of *brx* single mutants (Gujas et al., 2012; Kang et al., 2017; Mouchel et al., 2006) (Fig. 2D). Rather, both *jmj14* and *brx jmj14* responded like wild type (Fig. 2D).

To determine whether JMJ14 could regulate known players in protophloem differentiation, we performed RNA sequencing (RNAseq) of *jmj14* root tips. Applying a stringent cut-off (adjacent P-value<0.01), 1526 genes were found to be differentially expressed between *jmj14* and Col-0 (Table S1). This set displayed substantial overlap (>10-fold over random expectation) with RNAseq data from *bb* root tips that were monitored in parallel (Fig. 2E) (Table S2). Primary brassinosteroid-related or CLE45-related genes were, however, not differentially expressed, consistent with our physiological assays. Interestingly, the overlap with genes that were described to be H3K4 hypermethylated in *jmj14* seedlings (Ning

Development (2019) 146, dev183905. doi:10.1242/dev.183905

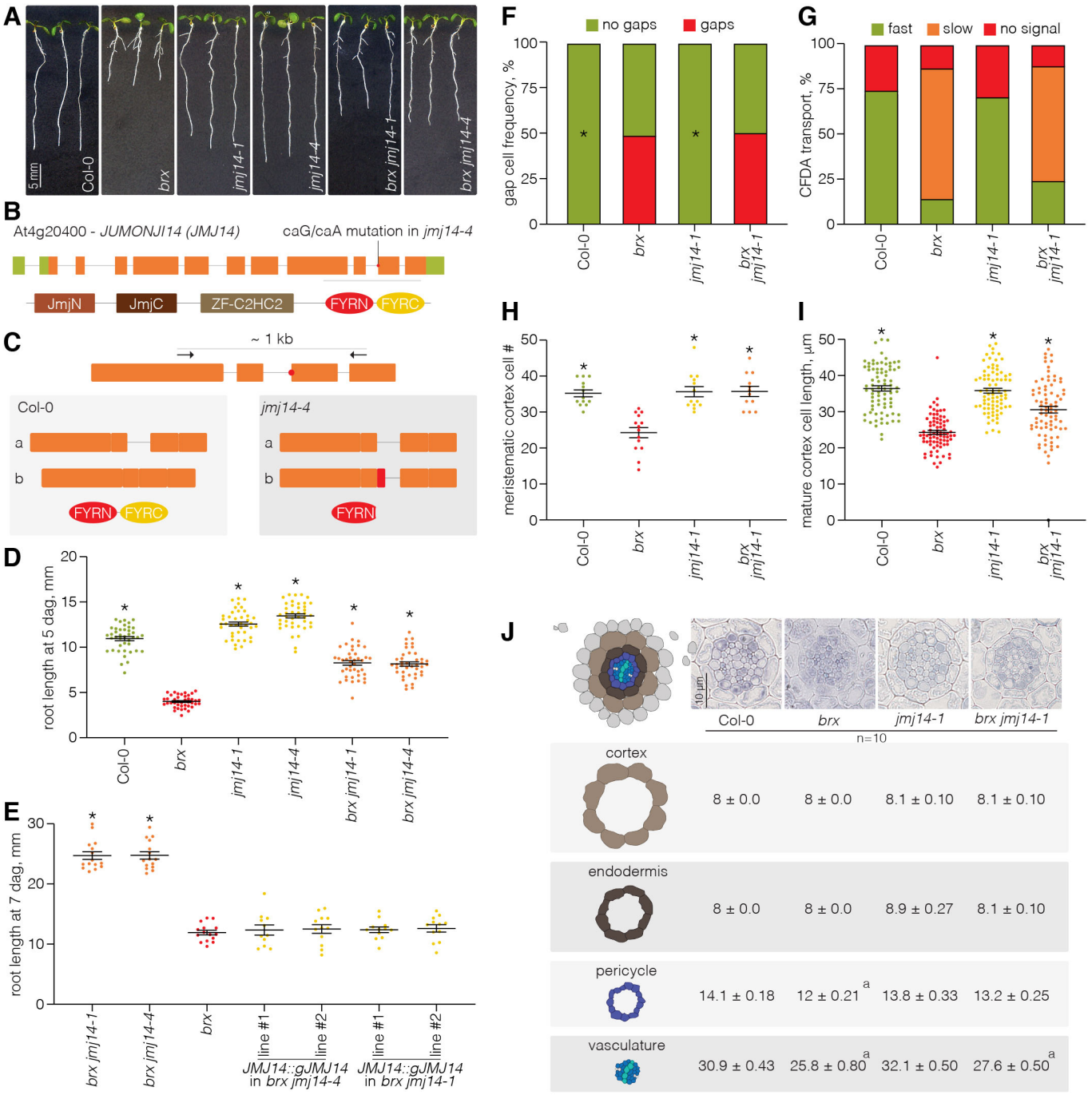

Fig. 1. *JMJ14* loss-of-function mutations partially suppress *brx* root phenotypes. (A) Representative 7-day-old seedlings of the indicated mutants grown in tissue culture, compared with the Col-0 wild-type control background. (B) Schematic of the *JMJ14* intron-exon structure (UTRs in green; coding sequences in orange), indicating the point mutation identified in the newly isolated *jmj14-4* allele (top), and the corresponding protein structure with its conserved domains (bottom). (C) Schematic of the partial *JMJ14* transcripts monitored in Col-0 and *jmj14-4*. 'a' represents the transcript before splicing of intron 10, 'b' the corresponding mature transcripts. Note that the intron is retained in *jmj14-4*, leading to a premature stop codon (red) at the end of the FYR-N domain. (D,E) Primary root length of indicated genotypes. (F) Gap cell frequency in root meristem protophloem strands of the indicated genotypes. (G) Classification of phloem-mediated CFDA dye translocation from the cotyledons of 4-day-old seedlings into the phloem unloading zone of the root tip. (H) Quantification of meristematic cortex cell number in the root meristems of 7-day-old seedlings of the indicated genotypes. (I) Mature cortex cell length in 7-day-old roots of the indicated genotypes. (J) Representative histological cross-sections of 6-day-old roots of the indicated genotypes, taken at the position where protoxylem has differentiated, and quantification of corresponding cell file numbers in different tissue layers. Statistically significant difference to Col-0 is indicated by 'a'. Plots display individual values (dots), the mean (wide bars) and the s.e.m. (whiskers). Statistically significant differences to *brx* are marked by asterisks; see Table S7 for statistical test details. dag, days after germination.

et al., 2015) was rather limited (Fig. S2A). However, unlike the essentially random overlap between H3K4-hypermethylated genes in *jmj14* seedlings and differentially expressed genes in *bb* (Fig. S2B), the corresponding overlap with genes that were upregulated in *jmj14* root tips was nearly 4-fold over random expectation (Fig. S2A). These genes could represent primary JMJ14 targets in the root (Table S3).

Development (2019) 146, dev183905. doi:10.1242/dev.183905

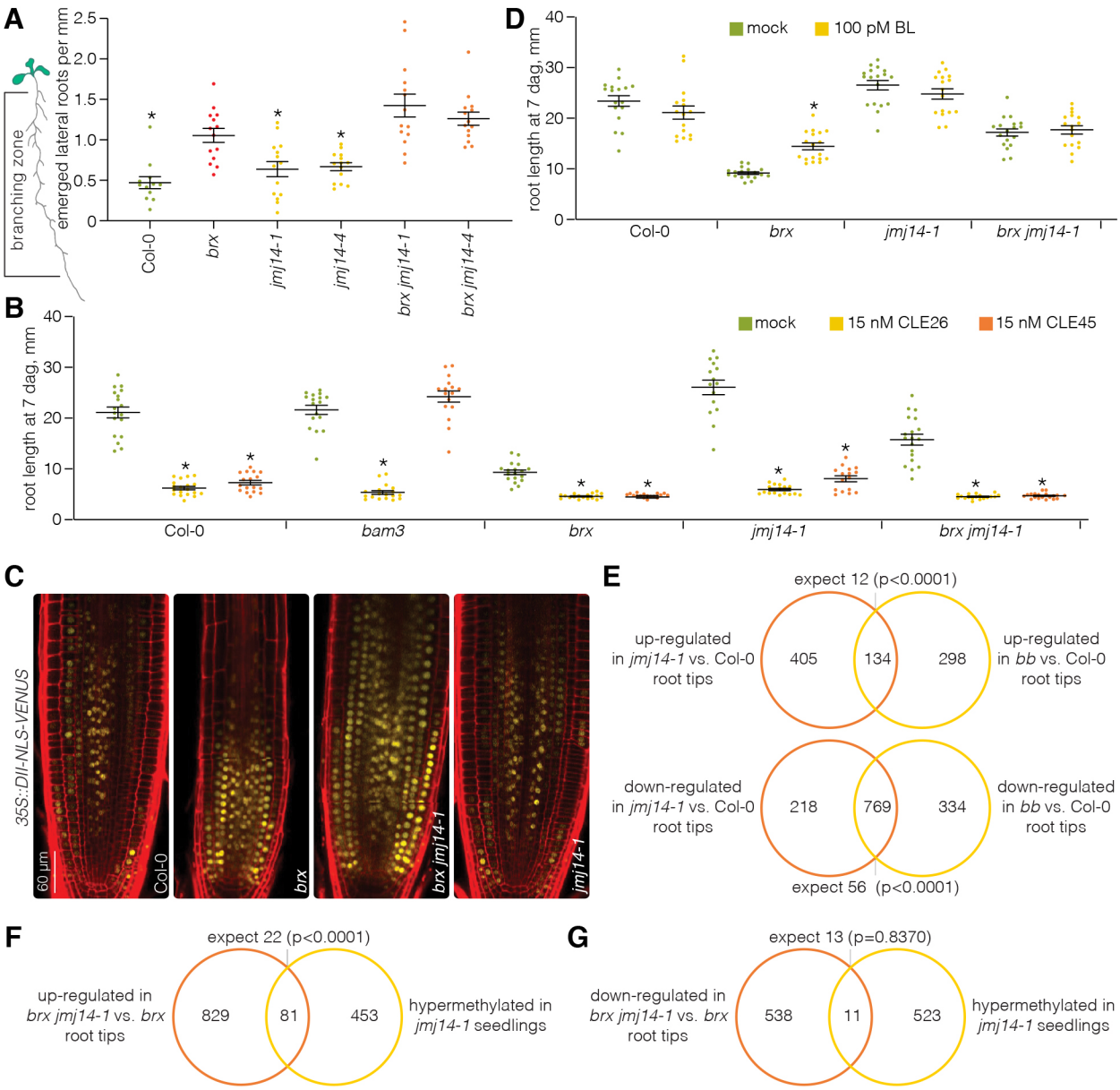

Fig. 2. *brx jmj14* double mutants retain physiological features of *brx*. (A) Lateral root density in12-day-old seedlings of the indicated genotypes. Diagram shows the root branching zone illustrated on a schematic seedling. (B) Root response of the indicated genotypes to CLE peptide application. (C) Auxin activity in the root meristems of 5-day-old roots of the indicated genotypes as monitored by the DII-VENUS inverse reporter (yellow fluorescence; note that higher fluorescence correlates with less auxin); composite images (red fluorescence is propidium iodide staining). (D) Root response of the indicated genotypes to brassinolide (BL) application. (E) Summary of the overlap between gene sets that were differentially expressed (adjacent *P*-value<0.01) in the root tips of the indicated mutants compared with Col-0 wild type. Statistical significance (Fisher's exact test) is indicated. See Tables S1 and S2 for gene lists. (F,G) Summary of the overlap between gene sets that were differentially expressed (adjacent *P*-value<0.01) in the root tips of *brx jmj14* compared with *brx*, with genes that were found to be H3K4 hypermethylated in *jmj14* seedlings. Statistical significance (Fisher's exact test) is indicated. See Tables S4 and S5 for details. Plots display individual values (dots), the mean (wide bars) and the s.e.m. (whiskers). Statistically significant differences to *brx* (A) or mock treatment (B,D) are marked by asterisks; see Table S7 for statistical test details. dag, days after germination.

However, known dominant suppressors of *brx*, through enhanced and/or ectopic expression (Breda et al., 2017; Briggs et al., 2006; Rodriguez-Villalon et al., 2014), were absent from the differentially expressed genes. To monitor pertinent changes directly, we performed another RNAseq experiment with *brx* and *brx jmj14* root tips. Again, many genes were differentially expressed between the two samples (n=1459) despite a stringent cut-off (adjacent *P*-value<0.01) (Table S4). Corroborating JMJ14 function, overlap between H3K4-hypermethylated genes in *jmj14* seedlings (Ning et al., 2015) and the 910 differentially expressed genes that were upregulated in *brx jmj14* double mutants was significant (Fig. 2F), whereas overlap with the 549 genes that were downregulated was random (Fig. 2G). Yet again, known suppressors of *brx* were found neither among these likely JMJ14 targets in the root (Table S5), nor among the wider set of differentially expressed genes. Finally, *brx* rescue by *jmj14* could not be explained by ectopic expression of the functional BRX homolog BRXL1, which we monitored by reporter gene assay (Fig. S3). In summary, our results suggest that *JMJ14* mutation partially rescues *brx* through pathways that are unrelated to those defined previously.

Development (2019) 146, dev183905. doi:10.1242/dev.183905

JMJ14 specificity resides in its FYR domain

To determine whether *JMJ14* is distinct from its homologs, as reported for flowering, we first monitored their expression by reporter constructs. NLS-3xVENUS fusion protein expressed under the control of different promoters indicated similar expression patterns and levels for *JMJ15*, *JMJ16* and *JMJ18* in the root vascular cylinder (Fig. 3A), similar to *JMJ14* (Fig. 3B). Moreover, available *jmj16* and *jmj18* T-DNA insertion loss-of-function mutants also did not display apparent root phenotypes (Fig. 3C,D). Yet, in *brx jmj16* and *brx jmj18* double mutants derived from crosses, *brx* root growth was barely alleviated (Fig. 3C,D). Because none of the homologs was differentially expressed in *jmj14* root tips, *JMJ14* therefore does not appear to act redundantly with *JMJ16* or *JMJ18* in the root. The premature stop codon in the *jmj14-4* allele pointed to a possible role of the FYR domain in diversification. To test this notion, we created transgenes that expressed the *JMJ14* coding region up to the FYR-N domain in fusion with a brief linker and different FYR domains under control of the *JMJ14* promoter (*JMJ14::JMJ14^{N}-14^{C}*, *JMJ14::JMJ14^{N}-16^{C}* and *JMJ14::JMJ14^{N}-18^{C}*) (Fig. 3E). Of these three constructs, only *JMJ14::JMJ14^{N}-14^{C}* was able to revert *brx jmj14-1* back to a *brx* phenotype (Fig. 3F), suggesting that *JMJ14::JMJ14^{N}-16^{C}* and *JMJ14::JMJ14^{N}-18^{C}* could not substitute for *JMJ14*. Thus, the FYR domain likely has a role in the functional diversification of this group of proteins and confers specificity to the action of JMJ14.

The *JMJ14* transcript region confers ubiquitous expression throughout the root

One intriguing finding from the expression analysis was that the *JMJ14* promoter is only active in already differentiating and mature stele cells, but not in the root meristem itself (Fig. 3B, Fig. 4A). This contrasted with the effects of *JMJ14* mutation on *brx* root meristems, which could not be explained by ectopic *JMJ14* expression in *brx* (Fig. 3B, Fig. 4B). Closer inspection indicated that the *JMJ14* promoter is active throughout the root vasculature, but not in the phloem, nor in Col-0 or *brx* (Fig. 4C,D, Movies 1 and 2). However, when the NLS-3xVENUS reporter protein was replaced by a fusion between the *JMJ14* coding sequence and CITRINE (*JMJ14::JMJ14-CITRINE*), the fusion protein was observed throughout the root (Fig. 4E,F). This pattern was not influenced by the presence or

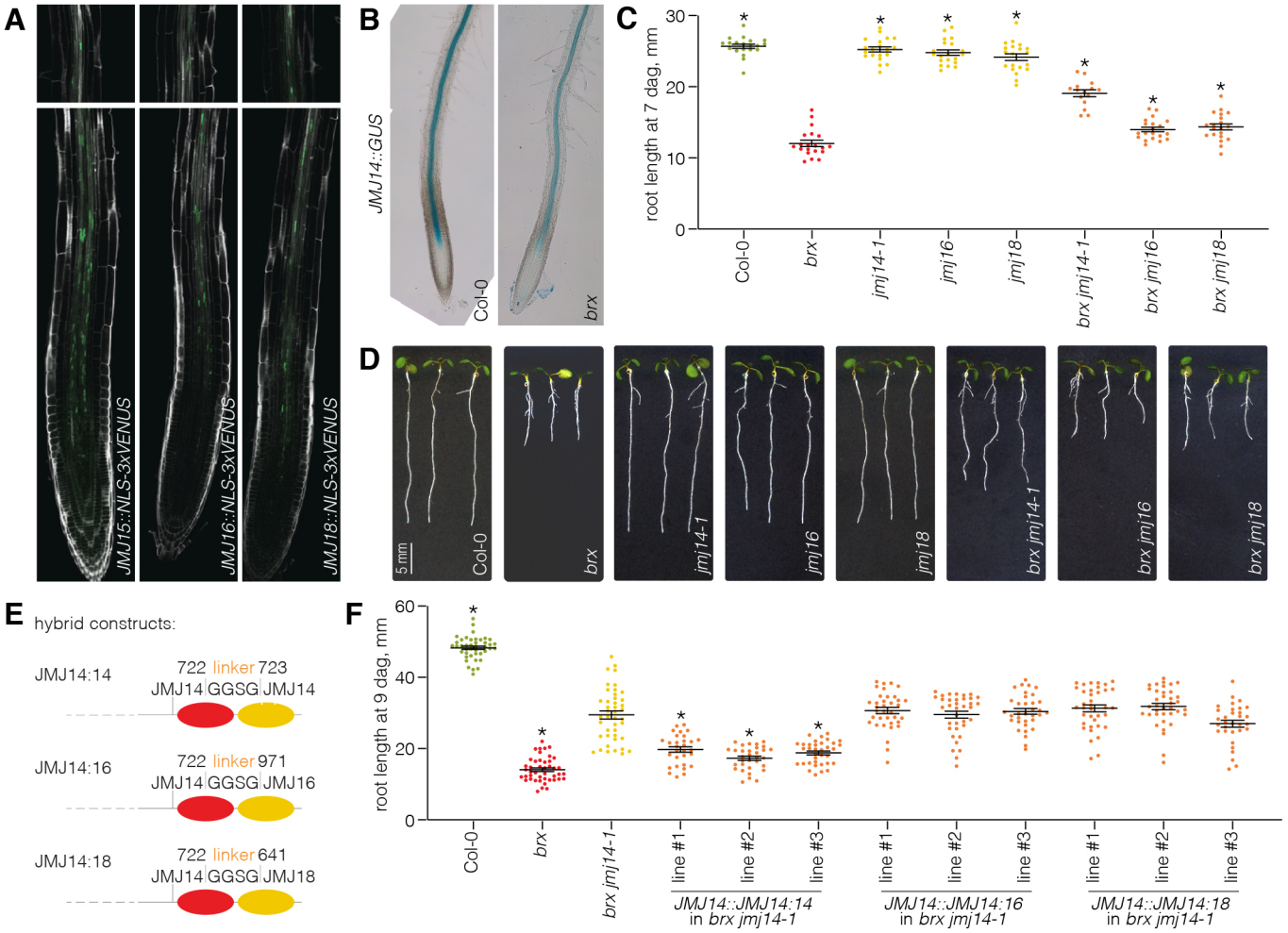

Fig. 3. JMJ14 specificity resides in its FYR domain. (A) Confocal microscopy images of root meristems (bottom) expressing the NLS-3XmVENUS reporter (green) under control of the indicated promoters, overlaid with Calcofluor White staining (gray). Top panels show snapshots of corresponding mature parts of the root. (B) Light microscopy images of GUS reporter staining (blue) for *JMJ14* promoter activity in 7-day-old roots of the indicated genotypes. (C) Root length of the indicated genotypes. (D) Representative 7-day-old seedlings of the indicated genotypes grown in tissue culture. (E) Schematic of hybrid JMJ protein constructs, indicating the amino acid position at the start of the corresponding FYR domains (red and yellow ovals). (F) Primary root length of the indicated genotypes. Plots display individual values (dots), the mean (wide bars) and the s.e.m. (whiskers). Statistically significant differences to *brx* (C) or *brx jmj14-1* (F) are marked by asterisks; see Table S7 for statistical test details. dag, days after germination.

Development (2019) 146, dev183905. doi:10.1242/dev.183905

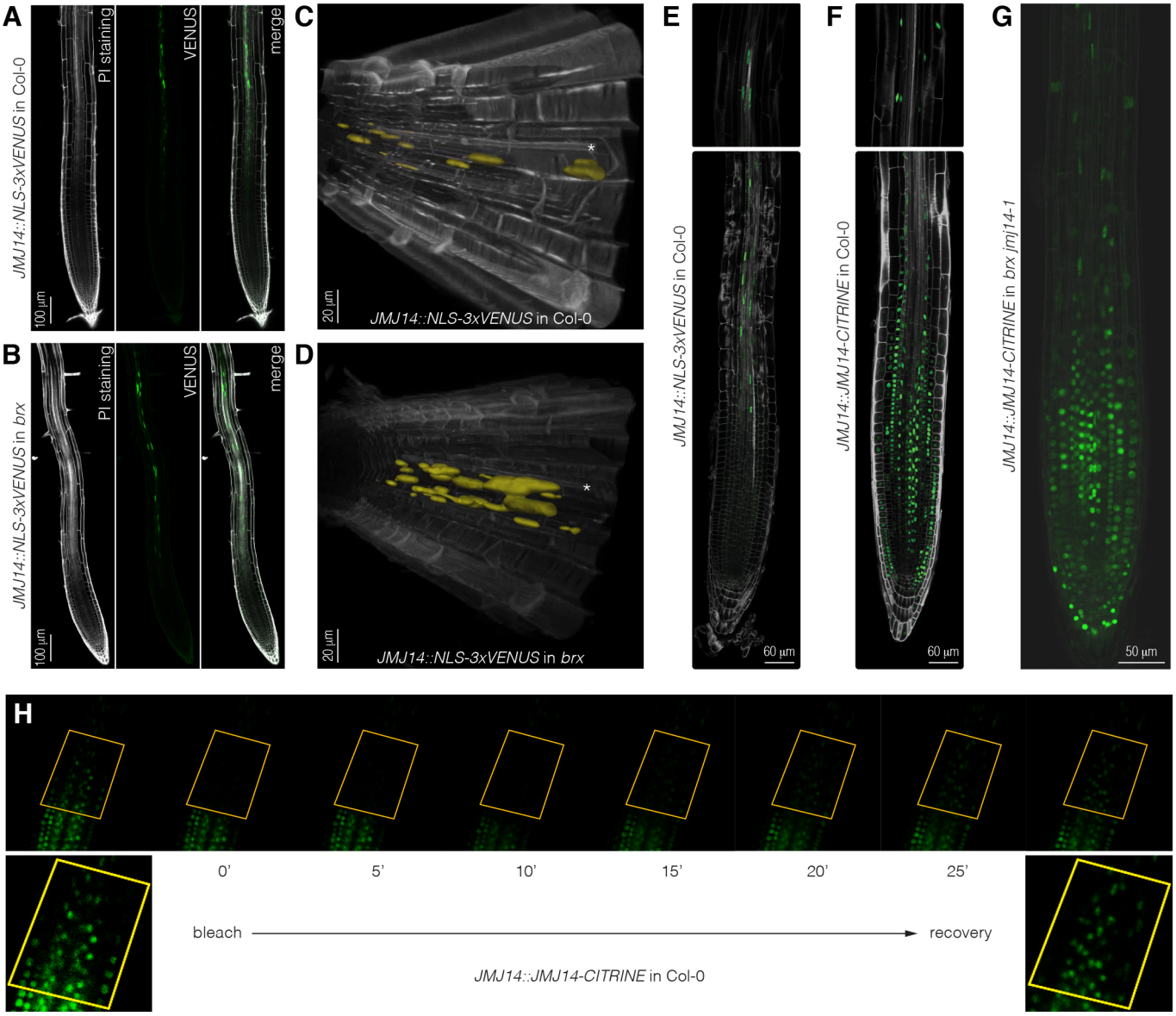

Fig. 4. The *JMJ14* transcript region contributes to its spatial expression pattern. (A,B) Confocal microscopy images of propidium iodide-stained root meristems (gray, left panels) expressing the NLS-3XmVENUS reporter (green, middle panels) under control of the *JMJ14* promoter (overlay, right panels) in Col-0 (A) or *brx* (B). (C,D) Three-dimensional reconstruction of *JMJ14* promoter activity (yellow) in the stele of Calcofluor White-stained Col-0 or *brx* roots (snapshots from corresponding Movies 1 and 2). Asterisks indicate phloem sieve element strands for orientation. (E,F) Confocal microscopy images of Calcofluor White-stained root meristems (gray) expressing either an NLS-3XmVENUS reporter protein (E) or a JMJ14-CITRINE fusion protein (F) (green) under control of the *JMJ14* promoter in Col-0. (G) Confocal microscopy images of root meristem expressing JMJ14-CITRINE fusion protein (green) under control of the *JMJ14* promoter in *brx*; overlay with light microscopy image. (H) Confocal microscopy images of a root meristem area expressing JMJ14-CITRINE fusion protein (green) under control of the *JMJ14* promoter in Col-0, following fluorescence recovery in the outlined trapezoid area after bleaching over time. Bottom panels show enlarged views of the images above.

absence of *BRX* (Fig. 4F,G). Transgenic expression of *JMJ14* coding sequence under control of the ubiquitous *UBQ10* promoter did not trigger any discernible gain-of-function phenotypes in Col-0 (Fig. S4A) and reverted the *brx jmj14* root phenotype (Fig. S4B), corroborating that ubiquitous JMJ14 expression is not detrimental and indicating that JMJ14 activity is well buffered, possibly by rate-limiting interacting factors.

Because of the strong nuclear localization of JMJ14-CITRINE and its ∼135 kDa size (∼108 kDa of JMJ14 plus ∼27 kDa of CITRINE), it seemed unlikely that the wider expression pattern was due to cell-to-cell protein movement. Indeed, in bleaching experiments, JMJ14-CITRINE expression was apparently recovered cell-autonomously, without any evidence for a gradient across the bleached area (Fig. 4H). Grafting experiments to determine whether *JMJ14* mRNA could be mobile indicated that this is not the case, in line with the finding that *JMJ14* was not among phloem-mobile transcripts identified in high-throughput approaches (Thieme et al., 2015; Yang et al., 2019). Collectively, our data therefore indicate that the transcript region of *JMJ14* contributes substantially to its expression pattern.

Conclusion

In summary, our study identified a hitherto unrecognized role of *JMJ14* in root development, which is evident in genetically

Development (2019) 146, dev183905. doi:10.1242/dev.183905

sensitized backgrounds. Our data suggest that this role is unique for JMJ14 compared with its homologs, and that this specificity is conferred by its FYR domain. Moreover, we show that cistronic sequences contribute to the *JMJ14* expression pattern, which might be of interest in light of previously reported JMJ14-dependent, supposedly non-cell-autonomous phenomena.

MATERIALS AND METHODS

Plant tissue culture, plant transformation, common Molecular Biology procedures [such as genomic DNA isolation, genotyping, (whole genome) sequencing], peptide treatments, phloem probe translocation, GUS staining, microscopy and physiological assays were performed according to standard procedures as previously described (Breda et al., 2017; Cattaneo and Hardtke, 2017; Depuydt et al., 2013; Kang et al., 2017; Kang and Hardtke, 2016).

Plant materials and growth conditions

For plant tissue culture, seeds were surface-sterilized, germinated and grown vertically on half strength Murashige & Skoog agar media with or without 0.3% sucrose under continuous light of ∼120 µE intensity at 22°C. All mutants were in the *A. thaliana* Columbia-0 (Col-0) wild-type background and, except the newly isolated *jmj14-4* allele, were described previously: *brx-2*, *jmj14-1* (SALK_135712), *jmj16-3* (SALK_029530), *jmj18-1* (SALK_073422) and *ops-2* (SALK_139316) (Liu et al., 2019; Lu et al., 2010; Rodrigues et al., 2009; Truernit et al., 2012; Yang et al., 2012b).

Transgene constructs

All DNA fragments were amplified from Col-0 genomic DNA or cDNA using suitable oligonucleotides (see Table S6). To monitor promoter activities, ∼2 kb fragments 5′ upstream of the *JMJ14* (At4g20400), *JMJ15* (At2g34880), *JMJ16* (At1g08620) and *JMJ18* (At1g30810) ATG start codons were cloned in front of an NLS-3xVENUS reporter in the pCAMBIA1305.1 plasmid. The genomic *JMJ14* fragment (including the promoter) was cloned into pCAMBIA1305.1 as well. The GUS reporter construct for the *JMJ14* promoter was created in pMDC163. The hybrid protein sequences expressed under control of the *JMJ14* promoter were cloned into plasmid pH7m24GW. The *JMJ14* coding sequence was fused to CITRINE and put under control of the *JMJ14* promoter by Gateway cloning of the three fragments into the pH7m34GW plasmid. The *UBQ10* promoter and *JMJ14* coding sequences were recombined into the pH7m24GW plasmid by Gateway cloning. The sequences of all DNA fragments are provided in the Table S6.

Evaluation of the *jmj14-4* point mutation effect

Seven-day-old roots of Col-0 and *jmj14-4* grown in parallel were harvested and frozen in liquid nitrogen before total RNA extraction was performed using a Qiagen RNeasy Plant kit. cDNA synthesis was performed as described previously (Depuydt et al., 2013). A ∼1 kb fragment spanning exons 9 to 12 was PCR-amplified using oligonucleotides 5′-CGAAGAA-AGTGGATGGTTGTTTAG-3′ and 5′-CACAGAAGTCCATGCATCAT-TAC-3′. The resulting DNA fragments were separated by gel electrophoresis, gel-extracted and Sanger sequenced directly.

RNA sequencing

For RNAseq, 7-day-old roots of the different genotypes (two independent replicates per genotype) grown in parallel on vertical plates were harvested and frozen in liquid nitrogen before total RNA extraction was performed using a Qiagen RNeasy Plant kit. cDNA synthesis, amplification, size selection, and high-throughput sequencing were performed on an Illumina HiSeq 2500 instrument (Col-0, *bb* and *jmj14*) or HiSeq 4000 instrument (*brx* and *brx jmj14*) (single read sequencing) as described previously (Depuydt et al., 2013; Rodriguez-Villalon et al., 2015). Bioinformatic analysis of the high-throughput sequencing data was performed with the HTS pipeline (David et al., 2014) (Col-0, *bb* and *jmj14*) or kallisto v.0.43.1 (Bray et al., 2016) followed by DESeq2 (Love et al., 2014) (*brx* and *brx jmj14*). The RNA sequencing raw data have been deposited in the SRA under accession numbers PRJNA559150 and PRJNA580217.

Quantitative real-time PCR (qPCR)

To determine *JMJ14* expression levels by qPCR, 5 mm root tips were collected from 7-day-old seedlings for total RNA extraction (Qiagen), and cDNAs were produced by reverse transcriptase (Invitrogen). q PCR was performed in triplicate (Table S7) using MESA Blue qPCR MasterMix (Eurogentec). *EF1a* was used as the reference gene (primers 5′-AAGGC-TCAAACGCCATCAAAGTTTTAAGAA-3′ and 5′-AGGTCACCAAGG-CTGCAGTGAAGAA-3′). *JMJ14* transcripts were quantified using primers 5′-AGTGTGCTTGACCCAACAA-3′ and 5′-AGCCCATTTATACTCTC-CAAAGG-3′.

Statistical analyses

Statistical analyses were performed in GraphPad Prism software version 8.2.0. Significance of differences was determined by one-way ANOVA with subsequent post-hoc Tukey test or Fisher's exact test. The analyses are provided together with the raw data in Table S7.

Acknowledgements

We would like to thank the Lausanne Genomic Technologies Facility for whole-genome sequencing and RNAseq services.

Competing interests

The authors declare no competing or financial interests.

Author contributions

Conceptualization: P.C., M.G., C.S.H.; Methodology: P.C., M.G.; Validation: P.C., M.G., P.M.; Formal analysis: P.C., M.G., C.S.H.; Investigation: P.C., M.G., P.M.; Writing - original draft: M.G., C.S.H.; Writing - review & editing: P.C.; Supervision: C.S.H.; Project administration: C.S.H.; Funding acquisition: C.S.H.

Funding

This work was supported by Swiss National Science Foundation (Schweizerischer Nationalfonds zur Förderung der Wissenschaftlichen Forschung) grants (31003A_166394 and 310030B_185379 to C.S.H.). M.G. was supported by a post-doctoral fellowship (GR 5009/1-1) from the Deutsche Forschungsgemeinschaft (DFG).

Data availability

RNA sequencing raw data have been deposited in the Sequence Read Archive under accession numbers PRJNA559150 and PRJNA580217.

Supplementary information

Supplementary information available online at
http://dev.biologists.org/lookup/doi/10.1242/dev.183905.supplemental

References

Anne, P. and Hardtke, C. S. (2017). Phloem function and development — biophysics meets genetics. *Curr. Opin. Plant Biol.* **43**, 22-28. doi:10.1016/j.pbi.2017.12.005

Bannister, A. J. and Kouzarides, T. (2005). Reversing histone methylation. *Nature* **436**, 1103-1106. doi:10.1038/nature04048

Bray, N. L., Pimentel, H., Melsted, P. and Pachter, L. (2016). Near-optimal probabilistic RNA-seq quantification. *Nat. Biotechnol.* **34**, 525-527. doi:10.1038/nbt.3519

Breda, A. S., Hazak, O. and Hardtke, C. S. (2017). Phosphosite charge rather than shootward localization determines OCTOPUS activity in root protophloem. *Proc. Natl. Acad. Sci. USA* **114**, E5721-E5730. doi:10.1073/pnas.1703258114

Breda, A. S., Hazak, O., Schultz, P., Anne, P., Graeff, M., Simon, R. and Hardtke, C. S. (2019). A cellular insulator against CLE45 peptide signaling. *Curr. Biol.* **29**, 2501-2508.e3. doi:10.1016/j.cub.2019.06.037

Briggs, G. C., Mouchel, C. F. and Hardtke, C. S. (2006). Characterization of the plant-specific BREVIS RADIX gene family reveals limited genetic redundancy despite high sequence conservation. *Plant Physiol.* **140**, 1306-1316. doi:10.1104/pp.105.075382

Cattaneo, P. and Hardtke, C. S. (2017). BIG BROTHER uncouples cell proliferation from elongation in the Arabidopsis primary root. *Plant Cell Physiol.* **58**, 1519-1527. doi:10.1093/pcp/pcx091

David, F. P. A., Delafontaine, J., Carat, S., Ross, F. J., Lefebvre, G., Jarosz, Y., Sinclair, L., Noordermeer, D., Rougemont, J. and Leleu, M. (2014). HTSstation: a web application and open-access libraries for high-throughput sequencing data analysis. *PLoS ONE* **9**, e85879. doi:10.1371/journal.pone.0085879

Depuydt, S., Rodriguez-Villalon, A., Santuari, L., Wyser-Rmili, C., Ragni, L. and Hardtke, C. S. (2013). Suppression of Arabidopsis protophloem differentiation

and root meristem growth by CLE45 requires the receptor-like kinase BAM3. *Proc. Natl. Acad. Sci. USA* **110**, 7074-7079. doi:10.1073/pnas.1222314110

Gan, E.-S., Xu, Y., Wong, J.-Y., Goh, J. G., Sun, B., Wee, W.-Y., Huang, J. and Ito, T. (2014). Jumonji demethylases moderate precocious flowering at elevated temperature via regulation of FLC in Arabidopsis. *Nat. Commun.* **5**, 5098. doi:10.1038/ncomms6098

García-Alai, M. M., Allen, M. D., Joerger, A. C. and Bycroft, M. (2010). The structure of the FYR domain of transforming growth factor beta regulator 1. *Protein Sci.* **19**, 1432-1438. doi:10.1002/pro.404

Greenberg, M. V. C., Deleris, A., Hale, C. J., Liu, A., Feng, S. and Jacobsen, S. E. (2013). Interplay between active chromatin marks and RNA-directed DNA methylation in Arabidopsis thaliana. *PLoS Genet.* **9**, e1003946. doi:10.1371/journal.pgen.1003946

Gujas, B., Alonso-Blanco, C. and Hardtke, C. S. (2012). Natural Arabidopsis brx loss-of-function alleles confer root adaptation to acidic soil. *Curr. Biol.* **22**, 1962-1968. doi:10.1016/j.cub.2012.08.026

Hazak, O., Brandt, B., Cattaneo, P., Santiago, J., Rodriguez-Villalon, A., Hothorn, M. and Hardtke, C. S. (2017). Perception of root-active CLE peptides requires CORYNE function in the phloem vasculature. *EMBO Rep.* **18**, 1367-1381. doi:10.15252/embr.201643535

Hong, E.-H., Jeong, Y.-M., Ryu, J.-Y., Amasino, R. M., Noh, B. and Noh, Y.-S. (2009). Temporal and spatial expression patterns of nine Arabidopsis genes encoding Jumonji C-domain proteins. *Mol. Cells* **27**, 481-490. doi:10.1007/s10059-009-0054-7

Jeong, J.-H., Song, H. R., Ko, J.-H., Jeong, Y.-M., Kwon, Y. E., Seol, J. H., Amasino, R. M., Noh, B. and Noh, Y.-S. (2009). Repression of FLOWERING LOCUS T chromatin by functionally redundant histone H3 lysine 4 demethylases in Arabidopsis. *PLoS ONE* **4**, e8033. doi:10.1371/journal.pone.0008033

Kang, Y. H. and Hardtke, C. S. (2016). Arabidopsis MAKR5 is a positive effector of BAM3-dependent CLE45 signaling. *EMBO Rep.* **17**, 1145-1154. doi:10.15252/embr.201642450

Kang, Y. H., Breda, A. and Hardtke, C. S. (2017). Brassinosteroid signaling directs formative cell divisions and protophloem differentiation in Arabidopsis root meristems. *Development* **144**, 272-280. doi:10.1242/dev.145623

Klose, R. J., Kallin, E. M. and Zhang, Y. (2006a). JmjC-domain-containing proteins and histone demethylation. *Nat. Rev. Genet.* **7**, 715-727. doi:10.1038/nrg1945

Klose, R. J., Yamane, K., Bae, Y., Zhang, D., Erdjument-Bromage, H., Tempst, P., Wong, J. and Zhang, Y. (2006b). The transcriptional repressor JHDM3A demethylates trimethyl histone H3 lysine 9 and lysine 36. *Nature* **442**, 312-316. doi:10.1038/nature04853

Ko, J.-H., Mitina, I., Tamada, Y., Hyun, Y., Choi, Y., Amasino, R. M., Noh, B. and Noh, Y.-S. (2010). Growth habit determination by the balance of histone methylation activities in Arabidopsis. *EMBO J.* **29**, 3208-3215. doi:10.1038/emboj.2010.198

Kouzarides, T. (2007). Chromatin modifications and their function. *Cell* **128**, 693-705. doi:10.1016/j.cell.2007.02.005

Le Masson, I., Jauvion, V., Bouteiller, N., Rivard, M., Elmayan, T. and Vaucheret, H. (2012). Mutations in the Arabidopsis H3K4me2/3 demethylase JMJ14 suppress posttranscriptional gene silencing by decreasing transgene transcription. *Plant Cell* **24**, 3603-3612. doi:10.1105/tpc.112.103119

Liu, P., Zhang, S., Zhou, B., Luo, X., Zhou, X. F., Cai, B., Jin, Y. H., Niu, D., Lin, J., Cao, X. et al. (2019). The histone H3K4 demethylase JMJ16 represses leaf senescence in Arabidopsis. *Plant Cell* **31**, 430-443. doi:10.1105/tpc.18.00693

Love, M. I., Huber, W. and Anders, S. (2014). Moderated estimation of fold change and dispersion for RNA-seq data with DESeq2. *Genome Biol.* **15**, 550. doi:10.1186/s13059-014-0550-8

Lu, F., Li, G., Cui, X., Liu, C., Wang, X.-J. and Cao, X. (2008). Comparative analysis of JmjC domain-containing proteins reveals the potential histone demethylases in Arabidopsis and rice. *J. Integr. Plant Biol.* **50**, 886-896. doi:10.1111/j.1744-7909.2008.00692.x

Lu, F., Cui, X., Zhang, S., Liu, C. and Cao, X. (2010). JMJ14 is an H3K4 demethylase regulating flowering time in Arabidopsis. *Cell Res.* **20**, 387-390. doi:10.1038/cr.2010.27

Lu, F., Cui, X., Zhang, S., Jenuwein, T. and Cao, X. (2011). Arabidopsis REF6 is a histone H3 lysine 27 demethylase. *Nat. Genet.* **43**, 715-719. doi:10.1038/ng.854

Lucas, W. J., Groover, A., Lichtenberger, R., Furuta, K., Yadav, S.-R., Helariutta, Y., He, X.-Q., Fukuda, H., Kang, J., Brady, S. M. et al. (2013). The plant vascular system: evolution, development and functions. *J. Integr. Plant Biol.* **55**, 294-388. doi:10.1111/jipb.12041

Mosammaparast, N. and Shi, Y. (2010). Reversal of histone methylation: biochemical and molecular mechanisms of histone demethylases. *Annu. Rev. Biochem.* **79**, 155-179. doi:10.1146/annurev.biochem.78.070907.103946

Mouchel, C. F., Osmont, K. S. and Hardtke, C. S. (2006). BRX mediates feedback between brassinosteroid levels and auxin signalling in root growth. *Nature* **443**, 458-461. doi:10.1038/nature05130

Ning, Y.-Q., Ma, Z.-Y., Huang, H.-W., Mo, H., Zhao, T.-T., Li, L., Cai, T., Chen, S., Ma, L. and He, X.-J. (2015). Two novel NAC transcription factors regulate gene expression and flowering time by associating with the histone demethylase JMJ14. *Nucleic Acids Res.* **43**, 1469-1484. doi:10.1093/nar/gku1382

Rodrigues, A., Santiago, J., Rubio, S., Saez, A., Osmont, K. S., Gadea, J., Hardtke, C. S. and Rodriguez, P. L. (2009). The short-rooted phenotype of the brevis radix mutant partly reflects root abscisic acid hypersensitivity. *Plant Physiol.* **149**, 1917-1928. doi:10.1104/pp.108.133819

Rodriguez-Villalon, A., Gujas, B., Kang, Y. H., Breda, A. S., Cattaneo, P., Depuydt, S. and Hardtke, C. S. (2014). Molecular genetic framework for protophloem formation. *Proc. Natl. Acad. Sci. USA* **111**, 11551-11556. doi:10.1073/pnas.1407337111

Rodriguez-Villalon, A., Gujas, B., van Wijk, R., Munnik, T. and Hardtke, C. S. (2015). Primary root protophloem differentiation requires balanced phosphatidylinositol-4,5-biphosphate levels and systemically affects root branching. *Development* **142**, 1437-1446. doi:10.1242/dev.118364

Saleh, A., Alvarez-Venegas, R., Yilmaz, M., Le, O., Hou, G., Sadder, M., Al-Abdallat, A., Xia, Y., Lu, G., Ladunga, I. et al. (2008). The highly similar Arabidopsis homologs of trithorax ATX1 and ATX2 encode proteins with divergent biochemical functions. *Plant Cell* **20**, 568-579. doi:10.1105/tpc.107.056614

Searle, I. R., Pontes, O., Melnyk, C. W., Smith, L. M. and Baulcombe, D. C. (2010). JMJ14, a JmjC domain protein, is required for RNA silencing and cell-to-cell movement of an RNA silencing signal in Arabidopsis. *Genes Dev.* **24**, 986-991. doi:10.1101/gad.579910

Shi, Y., Lan, F., Matson, C., Mulligan, P., Whetstine, J. R., Cole, P. A., Casero, R. A. and Shi, Y. (2004). Histone demethylation mediated by the nuclear amine oxidase homolog LSD1. *Cell* **119**, 941-953. doi:10.1016/j.cell.2004.12.012

Thieme, C. J., Rojas-Triana, M., Stecyk, E., Schudoma, C., Zhang, W., Yang, L., Miñambres, M., Walther, D., Schulze, W. X., Paz-Ares, J. et al. (2015). Endogenous Arabidopsis messenger RNAs transported to distant tissues. *Nat. Plants* **1**, 15025. doi:10.1038/nplants.2015.25

Truernit, E., Bauby, H., Belcram, K., Barthelemy, J. and Palauqui, J.-C. (2012). OCTOPUS, a polarly localised membrane-associated protein, regulates phloem differentiation entry in Arabidopsis thaliana. *Development* **139**, 1306-1315. doi:10.1242/dev.072629

Tsukada, Y.-I., Fang, J., Erdjument-Bromage, H., Warren, M. E., Borchers, C. H., Tempst, P. and Zhang, Y. (2006). Histone demethylation by a family of JmjC domain-containing proteins. *Nature* **439**, 811-816. doi:10.1038/nature04433

Yang, H., Han, Z., Cao, Y., Fan, D., Li, H., Mo, H., Feng, Y., Liu, L., Wang, Z., Yue, Y. et al. (2012a). A companion cell-dominant and developmentally regulated H3K4 demethylase controls flowering time in Arabidopsis via the repression of FLC expression. *PLoS Genet.* **8**, e1002664. doi:10.1371/journal.pgen.1002664

Yang, H., Mo, H., Fan, D., Cao, Y., Cui, S. and Ma, L. (2012b). Overexpression of a histone H3K4 demethylase, JMJ15, accelerates flowering time in Arabidopsis. *Plant Cell Rep.* **31**, 1297-1308. doi:10.1007/s00299-012-1249-5

Yang, L., Perrera, V., Saplaoura, E., Apelt, F., Bahin, M., Kramdi, A., Olas, J., Mueller-Roeber, B., Sokolowska, E., Zhang, W. et al. (2019). m^5C methylation guides systemic transport of messenger RNA over graft junctions in plants. *Curr. Biol.* **29**, 2465-2476.e5. doi:10.1016/j.cub.2019.06.042

Yu, X., Li, L., Li, L., Guo, M., Chory, J. and Yin, Y. (2008). Modulation of brassinosteroid-regulated gene expression by Jumonji domain-containing proteins ELF6 and REF6 in Arabidopsis. *Proc. Natl. Acad. Sci. USA* **105**, 7618-7623. doi:10.1073/pnas.0802254105